Lift forces on three-dimensional elastic and viscoelastic lubricated contacts

Arash Kargar-Estahbanati and Bhargav Rallabandi*
Department of Mechanical Engineering, University of California, Riverside, California 92521, USA

(Received 8 November 2020; accepted 22 February 2021; published 8 March 2021)

When an object suspended in fluid moves past a soft substrate it experiences an additional lift force due to the deformability of the substrate. In this work we find this lift force analytically for a general deformable substrate in the limit of small deformations. In particular we employ Lorentz's reciprocal theorem to obtain a general integral relation between the lift force and the linear response function of the soft substrate. We apply these results to an elastic layer, and discuss the behavior of the lift force as a function of Poisson's ratio and the thickness of the layer, obtaining analytic results for thin and thick layers. Then we generalize the theory to a linear viscoelastic response of the substrate. For oscillatory relative motion between the surfaces we find that the resulting lift force is a superposition of steady and oscillating modes whose amplitude and phase contain information about the elastic and viscous components of the material response. Our theory makes transparent the connection between the elastohydrodynamic lift force and the underlying response of the substrate and can be used to characterize the mechanical properties of an arbitrary soft material without solid-to-solid contact via lift force measurements.

DOI: 10.1103/PhysRevFluids.6.034003

I. INTRODUCTION

Lubrication flows with deformable boundaries (also known as soft lubrication) are widely encountered and studied in engineering [1], biophysics [2], and geophysics [3]. These flows has been studied in applications such as the rheology of polymer bearings [4], flows of cells in capillaries [5], the behavior of vesicles near walls [6], the collision of suspended particles [7], mechanics of earthquake and seismic faults [8], and mechanical characterization of soft surfaces [9–11]. The high pressure, small clearance and highly deformable surfaces in these applications result in a strong coupling between solid deformation and fluid pressure.

When a rigid symmetric object such as a sphere or a cylinder moves near a rigid wall at near-zero Reynolds number, the pressure is symmetric and no force normal to the wall (i.e., lift) is generated, due to reversibility of Stokes flow [12]. If the wall is compliant, however, the boundary deforms and generates an asymmetric pressure component that produces a nonzero lift force. For small deformations asymptotic approaches are often employed to approximate the lift force analytically [13–15]. In the past decade, various complexities in soft lubrication such as fluid compressibility [16], solid viscoelasticity [17], and the inertia of the fluid and the elastic medium [18] have been examined quantitatively. Other authors have studied the effects of electrostatic and van der Waals interactions [19], the effect of a background flow [20], or the effect of deformable channel boundaries on the flow of suspensions [21].

There are two broad classes of elastohydrodynamic lubrication problems involving parallel sliding between the surfaces [22]. The first involves pressing the object into the substrate, forcing the surfaces to initially make contact (the Hertz limit [23,24]). Then, a fluid film is established solely

*bhargav@engr.ucr.edu

due to relative motion between the surfaces [22,25,26]. For small velocities, the pressure in the thin film is controlled by boundary layers and results in (typically noninteger) power-law dependence of the lift force on the velocity [22,25,26]; see the review by Greenwood [27]. In the second class of problems, a finite clearance between the surfaces is maintained even in the absence of any relative motion [28,29]. This latter type of flow situation is non-Hertzian and can typically be analyzed with a regular perturbation in deformation, yielding a lift force that scales quadratically with velocity for small velocities. Here, we focus explicitly on this second situation, which is relevant for small normal loads [22] and has been validated in experimental settings involving macroscopic sliding and rolling cylinders [28,30] and microscopic noncontact rheometry [10,29].

Typically, the surfaces under lubrication are locally describable by a paraboloidal approximation involving two principal curvatures. Two-dimensional configurations (e.g., a cylindrical surface) nearby a soft wall have been analyzed extensively in past work [13,22,31,32] and often admit analytical solutions for small deformations. Corresponding three-dimensional versions of the problem (e.g., a locally spherical surface) are typically more complex to solve perturbatively so analysis of these problems has been restricted to some limiting cases. Urzay *et al.* [15] investigated the problem of a sphere moving parallel to a Winkler solid (applicable to thin, compressible elastic layers) using a perturbation expansion of the elastohydrodynamic Reynolds lubrication equation. More recently, Zhang *et al.* [29] provided a semianalytical solution for a fully incompressible thick elastic substrate, developing a small-deformation expansion and solving the resulting theory numerically at linear order in the deformation amplitude.

The recent experiments of Zhang *et al.* [29] measure the mean lift force on the oscillating probe tip of an atomic force microscope, in excellent agreement with their theory modeling the substrate as an elastic half-space. This suggests the use of lift forces for noncontact microrheometry of complex materials. However, as noted earlier, no theory exists that relates the underlying response of a complex material to the measured lift forces, except for the limiting cases of thin and thick elastic layers. Furthermore, oscillatory excitation (typical in microrheometry) may elicit a viscoelastic material response, further complicating the inference of a material response from a measured lift force.

In this work we develop a theory that addresses these points by directly relating lift forces and the material response, both for steady and oscillatory motion between the surfaces, for arbitrary linear responses of the underlying deformable substrate. The key feature that we build on is that the small-deformation lift force is linear in the solid deformation, even through it is nonlinear (specifically quadratic) in the fluid velocity. A consequence of this is that the force must be linearly related to the linear response function of the solid. We make this relation transparent by simplifying the problem of computing the force through the Lorentz reciprocal theorem [33], which leads to an integral involving the deformation of the substrate. Transforming this integral to Fourier space [34,35] lets us relate the deformation to the linear response function (i.e., the Green's function) of the substrate. This ultimately leads us to a general expression for the lift force in terms of the substrate Green's function.

We apply the formalism to the experimentally relevant situation where the soft substrate is composed of a linearly elastic material within finite thickness. In doing so we obtain the lift force due to an elastic layer with arbitrary thickness and Poisson ratio, recovering the results of Zhang *et al.* [29] and Urzay *et al.* [15] in the appropriate limits. We also resolve the question of how a nearly incompressible material (Poisson's ratio close to $1/2$) can appear compressible at small thicknesses and obtain results in agreement with the recent analysis of thin-film elasticity [36]. We then further develop the theory to account for the effect of substrate viscoelasticity on the lift force. For a laterally oscillating object, we show that the lift force is time dependent, and that different temporal Fourier modes of the lift force carry information about the storage and loss responses of the substrate.

The paper is arranged as follows: in Sec. II, we set up the problem and present scaling laws for small deformations. Section III develops the theoretical framework. Here, we first introduce the reciprocal theorem which forms one of core ideas behind this work, then present relevant results for

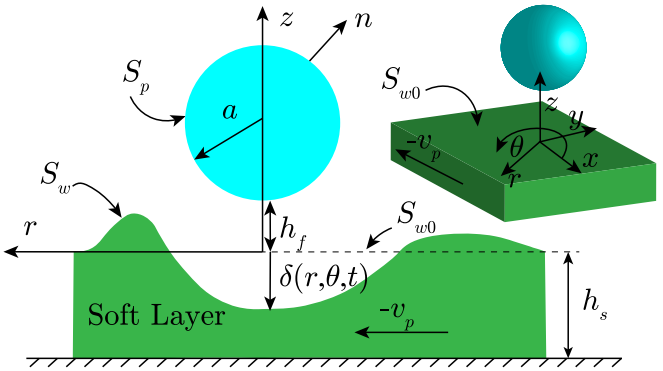

FIG. 1. A schematic of the problem: a sphere translates with negligible inertia in the lubrication limit ($h_f \ll a$) parallel to a soft layer. The pressure of the flow produces a small deformation of the layer, generating an elastohydrodynamic lift force. The problem is formulated in the a reference frame attached to the sphere.

the hydrodynamic fields, and finally obtain a general expression for the lift force due to an arbitrary linearly-responsive substrate. In Sec. IV, we apply the theory to steady-state motion past an elastic layer of finite thickness and discuss the dependence of the lift force for various combinations of layer thickness and Poisson's ratio, including asymptotic behaviors in the limits of thick and thin layers. We then focus on the case of oscillatory excitation near a viscoelastic substrate and detail the connection between the time-dependent lift force and the viscous and elastic components of the material response. We conclude in Sec. V.

II. SETUP OF THE PROBLEM

We consider a rigid sphere translating with velocity $\mathbf{v}_p = v_p(x,t)\mathbf{e}_x$ parallel to a nearby deformable substrate. The radius of the sphere is a and the smallest separation distance between the sphere and the undeformed wall is h_f. The sphere moves in a fluid with viscosity η and density ρ_f. We focus on small Reynolds number ($\rho_f v_p a/\eta \ll 1$) and assume that the flow is incompressible. In this case, we can disregard the effect of inertial forces compared with viscous forces and the governing equations in the fluid reduce to the Stokes equations

$$\nabla \cdot \mathbf{v} = 0 \quad \text{and} \quad \nabla \cdot \boldsymbol{\sigma}_f = \mathbf{0}, \tag{1}$$

where $\boldsymbol{\sigma}_f(\mathbf{x},t) = -p\mathbf{I} + \eta(\nabla\mathbf{v} + \nabla\mathbf{v}^T)$ is the stress at a point in the fluid defined using a pressure $p(\mathbf{x},t)$ and a fluid velocity $\mathbf{v}(\mathbf{x},t)$. We will also focus on the limit of narrow gaps ($h_f \ll a$) in which case normal stresses are dominated by pressure and the lubrication approximation is applicable.

The substrate is assumed to be soft and therefore deforms under the stresses of the flow. We model the substrate as a linearly elastic layer with thickness h_s, shear modulus μ, and Poisson's ratio ν that is mounted on a rigid base (Fig. 1). In Sec. IV B, we show that our main result is general to an arbitrary linear material response, including a linear viscoelastic response. We denote the vertical deformation of the top surface of the substrate by $\delta(\mathbf{x},t)$, where it is understood that the spatial dependence is on the coordinates (r,θ) in the plane of the undeformed surface.

It is convenient to formulate the problem in a reference frame that is attached to the sphere. By doing so, we measure the velocity of a perfectly rigid wall as $-\mathbf{v}_p$. Additionally, as depicted in Fig. 1, we set our origin on the undeformed wall and where it has the smallest clearance with the sphere. Thus, the deformed wall S_w is identified with $z = \delta(\mathbf{x},t)$. The deformability generates an extra

normal velocity component $w = \frac{D}{Dt}[\delta(\mathbf{x}, t)]$ where $\frac{D}{Dt} = \frac{\partial}{\partial t} + (\mathbf{v} \cdot \boldsymbol{\nabla})$ is the material derivative. Therefore, the no-slip boundary condition at the surfaces can be written as

$$\mathbf{v} = \mathbf{0} \quad \text{on} \quad S_p, \tag{2a}$$

$$\mathbf{v} = -\mathbf{v}_p - \left(\mathbf{v}_p \cdot \boldsymbol{\nabla}\delta - \frac{\partial \delta}{\partial t}\right)\mathbf{e}_z \quad \text{on} \quad S_w, \tag{2b}$$

where S_p and S_w represent the surface of the sphere and the deformed wall, respectively.

The deformation $\delta(\mathbf{x})$ is the vertical surface displacement of the solid under static equilibrium subject to surface pressure $p(\mathbf{x})$ exerted on it by the fluid. We note that the effect of tangential fluid stresses on the deformation of the solid are comparatively small in the lubrication limit $h_f \ll a$. We restrict our attention to small deformations ($\delta \ll h_s$) where linear elasticity is valid. Then, δ is most generally written in terms of a scalar Green's function $G(\mathbf{x})$ as

$$\delta(\mathbf{x}) = -\int p(\mathbf{y})\, G(\mathbf{x} - \mathbf{y})\, d^2\mathbf{y}, \tag{3}$$

where both $\mathbf{x}$ and $\mathbf{y}$ are on the undeformed surface of the solid, $z = 0$.

For a layer mounted on a rigid base, the Green's function is obtained from the point-forced solution to the equations of elasticity. We denote the displacement field in the (point-forced) solid by $\mathbf{u}(\mathbf{x}) = (u_x, u_y, u_z)$ and the corresponding stress tensor by $\boldsymbol{\sigma}_s = \mu(\boldsymbol{\nabla}\mathbf{u} + \boldsymbol{\nabla}\mathbf{u}^T) + \lambda(\boldsymbol{\nabla} \cdot \mathbf{u})\mathbf{I}$, where $\lambda = 2\mu\nu/(1 - 2\nu)$ is Lamé's first parameter. The displacement field is governed by mechanical equilibrium within the solid ($\boldsymbol{\nabla} \cdot \boldsymbol{\sigma}_s = \mathbf{0}$), subject to the boundary conditions

$$\mathbf{u} = \mathbf{0} \quad \text{at} \quad z = -h_s \quad \text{(the rigid base)}, \tag{4a}$$

$$\mathbf{n} \cdot \boldsymbol{\sigma}_s = \mathbf{n}\, \delta_{2D}(\mathbf{x}) \quad \text{at} \quad z = 0 \quad \text{(the undeformed top surface)}. \tag{4b}$$

The right side of Eq. (4b) corresponds to a point force in the $\mathbf{e_z}$ direction at the origin (note that $\mathbf{n} = \mathbf{e_z}$ on the $z = 0$ plane), where $\delta_{2D}(\mathbf{x})$ is the two-dimensional Dirac δ function. Thus, the Green's function is the vertical surface displacement of the solid: $G(\mathbf{x}) = u_z(z = 0)$. Note that δ is defined positive in regions where the solid is vertically dilated. Except for certain limiting cases, a simple closed-from expression for $G(\mathbf{x})$ cannot be found. Its Fourier transform, however, can be calculated analytically. We define the Fourier transform of a function in the xy plane $f(\mathbf{x})$ by $\hat{f}(\mathbf{q}') = \int_{\mathbb{R}^2} f(\mathbf{x}) e^{-i\mathbf{q}'\cdot\mathbf{x}} d^2\mathbf{x}$ and its inverse by $f(\mathbf{x}) = (2\pi)^{-2} \int_{\mathbb{R}^2} \hat{f}(\mathbf{q}') e^{i\mathbf{q}'\cdot\mathbf{x}} d^2\mathbf{q}'$, where $\mathbf{q}'$ is the wave-vector. Solving the equations of elasticity in the transformed space yields the Fourier transform of the Green's function [14,37]:

$$\tilde{G}(\mathbf{q}') = \frac{1 - \nu}{\mu\, q'}\left[\frac{(3 - 4\nu)\ \sinh(2q'h_s) - 2q'h_s}{(3 - 4\nu)\ \cosh(2q'h_s) + 2(q'h_s)^2 + 5 - 12\nu + 8\nu^2}\right], \tag{5}$$

where $q' = |\mathbf{q}'|$.

The system of Eqs. (1)–(3), (5) define the coupled nonlinear fluid-solid problem. In general, the real space Green's function must be computed by Fourier-inverting Eq. (5), and the result used in Eq. (4) to compute the deformation $\delta(\mathbf{x})$. Alternatively the convolution theorem may be used to recast Eq. (3) as $\tilde{\delta} = -\tilde{p}\tilde{G}$ (requiring the Fourier transform of p) and the result inverted to obtain $\delta(\mathbf{x})$. This nonlinear system can, in principle, be solved perturbatively, numerically or with a combination of the two, and the pressure integrated over the surface of the sphere to compute the lift force. In practice, however, the resulting integro-differential equation (see Refs. [25,29]) is generally not analytically solvable for three-dimensional surfaces, even for small deformations.

Before developing a detailed calculation of the lift force, it is useful to estimate its dependence on the physical parameters via a scaling analysis. The local geometry sets the characteristic horizontal length scale ℓ. For layers with $h_s \gtrsim \ell$, it is appropriate to using the scaling estimates $q' \sim 1/\ell$ and $q'h_s = O(1)$ in Eq. (5), so the characteristic scale of G is $1/(2\mu\ell)$ (the factor of 2 is used here for later convenience). In the limit of small deformations, the lubrication pressure scales like

$\eta v_p \ell / {h_f}^2$. Based on Eq. (3) and the scaling in Eq. (5), the deflection of solid layer scales as $\delta \sim p\ell/(2\mu)$, yielding the characteristic deformation scale $\delta_c \equiv \eta \ell^2 v_p / 2\mu {h_f}^2$. Thus, the deformation scale relative to the lubrication layer's thickness is

$$\frac{\delta_c}{h_f} = \frac{\eta\, \ell^2\, v_p}{2\mu\, {h_f}^3} \equiv \Lambda, \tag{6}$$

which could also be interpreted as dimensionless elastic compliance. In general, the elastohydrodynamic lift force F_L is a nonlinear function of Λ, see, e.g., [14,15]. For small Λ however, F_L is linear in Λ (or quadratic in v_p; this scaling typically holds for $\Lambda \lesssim 0.1$) and has the characteristic scale $F_L \sim \Lambda p \ell^2 \sim \Lambda \eta v_p \ell^3 / {h_f}^2 = v_p^2 \eta^2 \ell^5 / (\mu h_f^5)$ [14,29].

We note that the response of an elastic layer also depends on its normalized thickness $H_s = h_s/\ell = h_s/\sqrt{2ah_f}$. For very thin layers ($h_s \ll \ell$ or $H_s \ll 1$), the effective compliance (and thus the lift force) is smaller than the estimates above by factors of H_s [32,36]. Note that $H_s = h_s/\sqrt{2ah_f}$, so it is practical to explore a wide range of dimensionless thicknesses H_s in a single experiment, for example by changing the gap width h_f, instead of synthesizing layers with different thicknesses [38]. For other types of elastic substrates (e.g., thin flexible sheets), dimensionless compliances analogous to Eq. (6) that quantify the scale of $|\delta|/h_f$ can be inferred [34,35]. In all of these cases, the lift force is predicted to scale v_p^2 in the limit of deformations (small v_p). This is in agreement with measurements under a wide range of experimental conditions [28–30,35]. In the remaining sections, we will assume small deformations ($\Lambda \ll 1$) and focus solely on the leading contribution to the elastohydrodynamic lift force.

III. THEORY FOR THE LIFT FORCE

The usual approach for calculating the lift force in the soft lubrication problems is to first reduce the Stokes equations to the nonlinear Reynolds lubrication equation involving a pressure-dependent displacement. For small deformations ($\Lambda \ll 1$), the resulting equation may be solved using perturbation theory in powers of Λ. This procedure first involves calculating an approximation to the deformation $\delta(\mathbf{x})$, which is then used to calculate the perturbation to the pressure, which in turn is integrated to obtain the lift force. This approach has restricted analytic progress to a handful of limiting cases where $\delta(\mathbf{x})$ can be obtained in closed-form (viz. thin, compressible layers [15] and infinitely thick layers [29]) and even then the solution to the pressure perturbation may require numerical methods [29]. These issues are further complicated in the general situation, which additionally requires the (typically numerical) Fourier inversion of Eq. (5) to construct the Green's function.

A. Domain perturbation and the reciprocal theorem

Here, we use the Lorentz reciprocal theorem to circumvent these issues and make transparent the relation between the lift force and the underlying linear response function $G(\mathbf{x})$ of the material. We follow the analyses of Refs. [34,35] for elastic sheets, but ultimately find results for the lift force that generalize to any linear response—elastic or inelastic—of the soft material. Since the solid deformation is small compared with the sphere-wall clearance ($\Lambda \ll 1$), we can approximate the velocity on the deformable wall using a perturbative expansion about the undeformed wall location S_{w0} ($z = 0$). The left side of Eq. (1b) can be approximated as $(\mathbf{v} + \delta \partial \mathbf{v}/\partial z)|_{z=0}$ up to terms of $O(\delta^2)$. Rearranging yields an effective velocity condition at the undeformed wall location S_{w0}, which reads

$$\mathbf{v} = -\mathbf{v}_p - \left(\mathbf{v}_p \cdot \nabla\delta - \frac{\partial \delta}{\partial t}\right)\mathbf{e}_z - \delta \frac{\partial \mathbf{v}}{\partial z} + O\left(\frac{\delta^2}{2}\frac{\partial^2 \mathbf{v}}{\partial z^2}\right) \quad \text{on} \quad S_{w0}. \tag{7}$$

Recall that $\delta \propto \Lambda h_f$. Since we only focus on the leading-order lift force (linear in the deformation amplitude) we disregard all correction terms of $O(\Lambda^2)$.

The reciprocal theorem relates integral properties of the flow of interest (the main flow) to those of another "model" Stokes flow. Since we are interested in the lift force on the sphere, we choose the model flow to correspond to the translation of the same sphere perpendicular to a rigid wall with velocity $\hat{\mathbf{v}}_p = \hat{v}_p \mathbf{e_z}$. The reciprocal theorem, applied to the undeformed fluid volume, states that

$$\int_{S_p+S_{w0}+S_\infty} \mathbf{n}\cdot\boldsymbol{\sigma}\cdot\hat{\mathbf{v}}\, dS = \int_{S_p+S_{w0}+S_\infty} \mathbf{n}\cdot\hat{\boldsymbol{\sigma}}\cdot\mathbf{v}\, dS\,, \tag{8}$$

where $\mathbf{n}$ is the normal vector directed into the fluid. With the domain projection in (7), both the model problem ($\hat{\boldsymbol{\sigma}}, \hat{\mathbf{v}}$) and the domain-perturbed main problem ($\boldsymbol{\sigma}, \mathbf{v}$) are Stokes flows now defined in a domain enclosed by S_p (the sphere), S_{w0} (undeformed wall) and S_∞ (bounding surface at infinity). The integral over S_p vanishes identically in a reference frame attached to the sphere. Observing that $\mathbf{n} = \mathbf{e}_z$ on the undeformed wall and using $\hat{\mathbf{v}}_p = \hat{v}_p\,\mathbf{e}_z$ on S_{w0} and S_∞, (8) can be written explicitly as

$$F_L\hat{v}_p = \hat{\mathbf{F}}\cdot\mathbf{v}_p - \int_{S_{w0}} \mathbf{e}_z\cdot\widehat{\boldsymbol{\sigma}}\cdot\left[\left(\mathbf{v}_p\cdot\nabla\delta - \frac{\partial\delta}{\partial t}\right)\mathbf{e}_z + \delta\frac{\partial\mathbf{v}}{\partial z} + O\left(\frac{\delta^2}{2}\frac{\partial^2\mathbf{v}}{\partial z^2}\right)\right]dS, \tag{9}$$

where $F_L = \int_{S_p} \mathbf{n}\cdot\boldsymbol{\sigma}\cdot\mathbf{e}_z\, dS$ is the hydrodynamic lift force on the sphere in the main problem, $\hat{\mathbf{F}} = \int_{S_p} \mathbf{n}\cdot\hat{\boldsymbol{\sigma}}$ is the hydrodynamic force in the model problem, and $\mathbf{v}_p = v_p\mathbf{e}_x$. Equation (9) circumvents the complexities in obtaining the detailed $O(\Lambda)$ pressure and velocities to obtain the lift force. We evaluate Eq. (9) in Sec. III C after first describing the model and main flow problems below.

B. Approximations to the main and model flows

To the level of approximation used in Eq. (9), it suffices to approximate $\partial\mathbf{v}/\partial z$ with the flow due to a sphere translating parallel to a rigid wall. This is the leading [i.e., $O(\Lambda^0)$] approximation to force in the full elastohydrodynamic problem at hand. The solution of both the leading-order main flow and the model flow are well-known and are thoroughly described in the literature [39,40], so we only discuss them briefly here. As discussed earlier, we focus on the limit of $h_f \ll a$ where lubrication theory is valid, and normalize horizontal lengths by the characteristic length scale $\ell = \sqrt{2ah_f}$ and distances across the gap by the gap width h_f. We define the dimensionless polar coordinates (R, θ, Z) such that $R = r/\ell$ and $Z = z/h_f$ with $x = r\cos\theta$ and $y = r\sin\theta$, cf. Fig. 1. The sphere profile S_p is approximated by a parabola $Z = H(R) = 1 + R^2$, where $R = 0$ represents the nearest point of the sphere to the wall.

1. Model problem

The model problem describes the motion of a sphere normal to a rigid wall in a Stokes flow. We introduce dimensionless velocity and pressure fields

$$\hat{V}_r = \frac{\hat{v}_r}{\hat{v}_p}\frac{\ell}{h}, \quad \hat{P} = \frac{\hat{p}}{p_\perp}, \tag{10}$$

where $\hat{V}_r$ is the radial component of the flow velocity and $p_\perp = \frac{\eta\hat{v}_p\,\ell^2}{{h_f}^3}$ is the characteristic pressure scale. The solutions are well known [41,42] and are given by

$$\hat{P} = -\frac{3}{2(1+R^2)^2}, \tag{11a}$$

$$\hat{V}_r = \frac{1}{2}\frac{\partial\hat{P}}{\partial R}Z[Z - H(R)]. \tag{11b}$$

Due to the symmetry of the flow about Z axis, the azimuthal velocity $\hat{V}_\theta = 0$. From the equation above we find

$$\left.\frac{\partial \hat{V}_r}{\partial Z}\right|_{Z=0} = -\frac{3R}{(1+R^2)^2}. \tag{12a}$$

We employ these results later in the model problem stress tensor $\hat{\boldsymbol{\sigma}}$.

2. Leading approximation to the main problem

The solution to the main problem (sphere translating parallel to a soft elastic layer) can be expressed, in principle, in a power series in Λ for $\Lambda \ll 1$. As discussed in the previous section, we are only concerned with the leading order lift force, linear in the deformation amplitude. The reciprocal relation Eq. (21a) isolates these linear terms explicitly, so we only require the solution to the main problem accurate to $O(\Lambda^0)$ to obtain a force accurate to $O(\Lambda)$; cf. [32] for a formal perturbation expansion. Physically, this leading-order solution corresponds to the parallel motion of a sphere near a rigid wall.

We normalize the velocity and pressure of the flow with v_p and $p_\parallel = \frac{\eta v_p \ell}{{h_f}^2}$, respectively, and define the dimensionless variables

$$V_r = \frac{v_r}{v_p}, \quad V_\theta = \frac{v_\theta}{v_p}, \quad P = \frac{p}{p_{||}}. \tag{13}$$

Contrary to wall-normal motion, the flow in the main problem is not axisymmetric and V_θ is nonzero. The solution to the $O(\Lambda^0)$ main problem is well known [12], so we only report the relevant results,

$$P = \frac{6R}{5(1+R^2)^2}\cos\theta, \tag{14a}$$

$$V_r = \frac{1}{2}\frac{\partial P}{\partial R}Z[Z - H(R)] + \left(\frac{Z}{H(R)} - 1\right)\cos\theta, \tag{14b}$$

$$V_\theta = \frac{1}{2}\frac{1}{R}\frac{\partial P}{\partial \theta}Z[Z - H(R)] - \left(\frac{Z}{H(R)} - 1\right)\sin\theta, \tag{14c}$$

valid up to terms of $O(\Lambda)$. From the above solutions, one finds

$$\left.\frac{\partial V_r}{\partial Z}\right|_{Z=0} = \frac{2}{5}\frac{1+7R^2}{(1+R^2)^2}\cos\theta, \tag{15a}$$

$$\left.\frac{\partial V_\theta}{\partial Z}\right|_{Z=0} = -\frac{2}{5}\frac{\sin\theta}{1+R^2}. \tag{15b}$$

C. Evaluating the lift force integral

We now use the results of the previous section to evaluate Eq. (9). The first term at the right-hand side of Eq. (9) vanishes since $\hat{\mathbf{F}}_L$ is orthogonal to $\mathbf{v}_p$. Using Eq. (10), the traction $\mathbf{e}_z \cdot \hat{\boldsymbol{\sigma}}$ in Eq. (9) can be expressed as

$$\mathbf{e}_z \cdot \hat{\boldsymbol{\sigma}}|_{z=0} = \frac{\eta \hat{v}_p \ell^2}{{h_f}^3}\left(-\hat{P}\,\mathbf{e}_z + \frac{h_f}{\ell}\frac{\partial \hat{V}_r}{\partial Z}\mathbf{e}_r\right)\Bigg|_{Z=0}. \tag{16}$$

The scaling analysis of Sec. II suggests a deflection scale $\delta_c = \eta v_p \ell^2/2\mu\, {h_f}^2$, which motivates a dimensionless deflection $\Delta(\mathbf{X}, \mathbf{T}) = \delta(\mathbf{x}, \mathbf{t})/\delta_\mathbf{c}$, where $T = t v_p/\ell$ is the rescaled time. Substituting

this definition into Eq. (9), the general expression for the lift force is found to be

$$F_L = -\frac{\eta^2 {v_p}^2 \ell^5}{2\mu {h_f}^5} \int_0^{2\pi} \int_0^{\infty} \left[\hat{P} \frac{\partial \Delta}{\partial T} - \hat{P} \left(\frac{\partial \Delta}{\partial R} \cos\theta - \frac{1}{R} \frac{\partial \Delta}{\partial \theta} \sin\theta \right) + \Delta \frac{\partial \hat{V}_r}{\partial Z} \frac{\partial V_r}{\partial Z} \right] \Bigg|_{Z=0} R\, dR\, d\theta. \tag{17}$$

The above expression is asymptotic to linear order in the deformation for arbitrary deformations $\Delta(\mathbf{X})$ in the lubrication limit. Defining the dimensionless Green's function $\mathcal{G} = 2\mu\ell G$, the deformation is related to the pressure by

$$\Delta(\mathbf{X}) = -\int_{\mathbb{R}^2} P(\mathbf{Y})\, \mathcal{G}(\mathbf{X} - \mathbf{Y}) d^2\mathbf{Y}. \tag{18}$$

For time-dependent motion of the sphere, transients decay over the characteristic timescale ℓ/v_p. Below we assume that the motion of the sphere is steady, so Δ is time-independent in the frame of reference attached to the sphere. This assumption is relaxed in the Sec. IV B.

In principle Eq. (18), supplemented by the appropriate Green's function and with the results of Sec. III B, provides all the necessary information to evaluate the lift force using Eq. (17). However, this calculation remains difficult in practice since the Green's function is only known in Fourier space. Rather than trying to evaluate the real-space Green's function, we transform the integral Eq. (17) to Fourier space. To this end it is useful to define a dimensionless Fourier variable $\mathbf{q} = \mathbf{q}'\ell$ [polar representation $(q,\ \varphi)$] and the Fourier transform of the Green's function $\tilde{\mathcal{G}}(\mathbf{q}) = 2\mu\tilde{G}(\mathbf{q}')/\ell$. Using the convolution theorem, the integral relation Eq. (18) transforms as

$$\tilde{\Delta}(\mathbf{q}) = -\tilde{P}(\mathbf{q})\, \tilde{\mathcal{G}}(\mathbf{q}). \tag{19}$$

Next, we invoke Parseval's integral theorem,

$$\int_{R^2} f_1(\mathbf{X}) f_2(\mathbf{X}) d^2\mathbf{X} = \frac{1}{(2\pi)^2} \int_{R^2} \tilde{f}_1(\mathbf{q}) [\tilde{f}_2(\mathbf{q})]^* d^2\mathbf{q}, \tag{20}$$

where $f_1(\mathbf{X})$ and $f_2(\mathbf{X})$ are real-valued functions and the asterisk denotes the complex conjugate. Applying Eq. (20) to Eq. (17), the steady-state lift force on the sphere can be expressed as an integral over Fourier space as

$$F_L = -\frac{\eta^2 {v_p}^2 \ell^5}{8\pi^2 \mu {h_f}^5} \int_0^{2\pi} \int_0^{\infty} \left(-\tilde{\hat{P}}(iq\tilde{\Delta}\cos\varphi)^* + \widetilde{\frac{\partial \hat{V}_r}{\partial Z} \frac{\partial V_r}{\partial Z}} \tilde{\Delta}^* \right) \Bigg|_{Z=0} q\, dq\, d\varphi \tag{21a}$$

$$= \frac{\eta^2 {v_p}^2 \ell^5}{8\pi^2 \mu {h_f}^5} \int_0^{2\pi} \int_0^{\infty} \left(i\tilde{\hat{P}} q \cos\varphi + \widetilde{\frac{\partial \hat{V}_r}{\partial Z} \frac{\partial V_r}{\partial Z}} \right) \tilde{P}^* \tilde{\mathcal{G}}^* \Bigg|_{Z=0} q\, dq\, d\varphi. \tag{21b}$$

Here, we used the relations $\cos\theta\, \partial\Delta/\partial R - R^{-1} \sin\theta\, \partial\Delta/\partial\theta = \partial\Delta/\partial X$ and $\widetilde{(\partial\Delta/\partial X)} = i\, q \cos\varphi\, \tilde{\Delta}$, along with Eq. (19).

Finally, we calculate (using Mathematica) the Fourier transforms of P, $\hat{P}$ and $\frac{\partial \hat{V}_r}{\partial Z} \frac{\partial V_r}{\partial Z}$ (cf. Sec. III B) to find

$$\tilde{P} = -\frac{6\pi}{5} iqK_0(q) \cos\varphi, \tag{22a}$$

$$\tilde{\hat{P}} = -\frac{3\pi}{2} qK_1(q), \tag{22b}$$

$$\widetilde{\frac{\partial \hat{V}_r}{\partial Z} \frac{\partial V_r}{\partial Z}} = -\frac{3\pi}{10} iq^2 [qK_0(q) - 5K_1(q)] \cos\varphi, \tag{22c}$$

where K_0 is the modified Bessel function of the second kind. After substituting the above results and using $\ell = \sqrt{2ah_f}$, Eq. (21a) yields a general expression for the steady-state force,

$$F_L = \frac{9\,\eta^2 {v_p}^2\, a^{\frac{5}{2}}}{25\sqrt{2}\,\mu\, {h_f}^{\frac{5}{2}}} \int_0^\infty \int_0^{2\pi} q^5 \{K_0(q)\}^2 \tilde{\mathcal{G}}^*(\mathbf{q}) \cos^2\varphi \, d\varphi \, dq. \tag{23}$$

The same steps allow for a similarly compact representation for the lift on a cylinder (see the Appendix). Note that [34,35] used a similar approach to analyze the normal motion of a sphere near an elastic sheet.

Equation (23) presents the most general form of the steady-state lift force on a rigid sphere translating parallel to any linearly deformable substrate with a small clearance. We note that nowhere in the development of this result have we used the specific form of $\tilde{\mathcal{G}}$, so Eq. (23) applies to any steady-state linear response of the soft material, providing a direct link between the lift force and the substrate response. Furthermore, in most systems, including for thin elastic layers, the response function is typically only known (indeed, derived) in Fourier space, with the real-space counterparts being available only in limiting cases. Additionally, the kernel $q^5\{K_0(q)\}^2$ is everywhere bounded and decays exponentially, making integration of Eq. (23) analytically tractable and numerically efficient for practically relevant response functions $\tilde{\mathcal{G}}$. Contrast this with an approach involving computing Δ directly in real space, for which the integral converges much more slowly or may even diverge [34,43,44]. Finally, the present approach provides a powerful and convenient route to the elastohydrodynamic lift even when the material response in anisotropic ($\tilde{\mathcal{G}}$ depends on both q and φ), e.g., graded materials [45,46].

IV. DISCUSSION

A. Steady state force on a sphere near a finite-thickness elastic layer

We now use Eq. (23) to analyze the lift force due to a linearly elastic layer, introduced in Sec. II. Past work has focused on either the limits of thin or thick layers or on the limit of incompressible materials for cylinders [14]. Here, we analyze the force for a layer of arbitrary thickness and Poisson's ratio. We discuss the applicability of the Winkler model (often favored for its simplicity but becoming degenerate for incompressible materials) for nearly incompressible thin elastic layers.

For a layer of dimensionless thickness $H_s = h_s/\ell$, the (dimensionless) Fourier transform $\tilde{\mathcal{G}} = 2\mu\tilde{G}/\ell$ is [see Eq. (5)]

$$\tilde{\mathcal{G}}(\mathbf{q}) = \frac{2(1-\nu)}{q}\left[\frac{(3-4\nu)\sinh(2qH_s) - 2qH_s}{(3-4\nu)\cosh(2qH_s) + 2(qH_s)^2 + 8\nu^2 - 12\nu + 5}\right]. \tag{24}$$

Substituting the above result into Eq. (23) and evaluating the φ integral yields

$$F_L = \frac{18\pi}{25\sqrt{2}} F_{L0} \int_0^\infty q^4 K_0(q)^2 \, \frac{(1-\nu)\{(3-4\nu)\sinh(2qH_s) - 2qH_s\}}{(3-4\nu)\cosh(2qH_s) + 2(qH_s)^2 + 8\nu^2 - 12\nu + 5}\, dq, \tag{25}$$

where $F_{L0} = \eta^2 {v_p}^2\, a^{\frac{5}{2}}/(\mu\, {h_f}^{\frac{5}{2}})$ is the characteristic elastohydrodynamic lift force scale. The above integral for the lift force is evaluated numerically and the result is plotted as a function of H_s for various values of Poisson's ratio in Fig. 2(a). As one may observe, by increasing the thickness, the lift force converges to a finite value corresponding to an infinitely thick layer.

By replacing the general Green's function in Eq. (23) with its infinite-thickness limit [$\tilde{\mathcal{G}}(H_s \to \infty) = 2(1-\nu)/q$], the limiting value of the lift force is found to be

$$F_L(H_s \to \infty) = \frac{\eta^2 {v_p}^2\, a^{\frac{5}{2}}}{\mu\, {h_f}^{\frac{5}{2}}} \frac{243\,\pi^3}{6400\sqrt{2}}(1-\nu). \tag{26}$$

For an incompressible material ($\nu = 1/2$), the dimensionless lift force F_L/F_{L0} reduces to $\frac{243\pi^3}{12800\sqrt{2}} \simeq 0.416$, which is the prefactor found in Zhang *et al.* [29] from a numerical solution of the $O(\Lambda)$

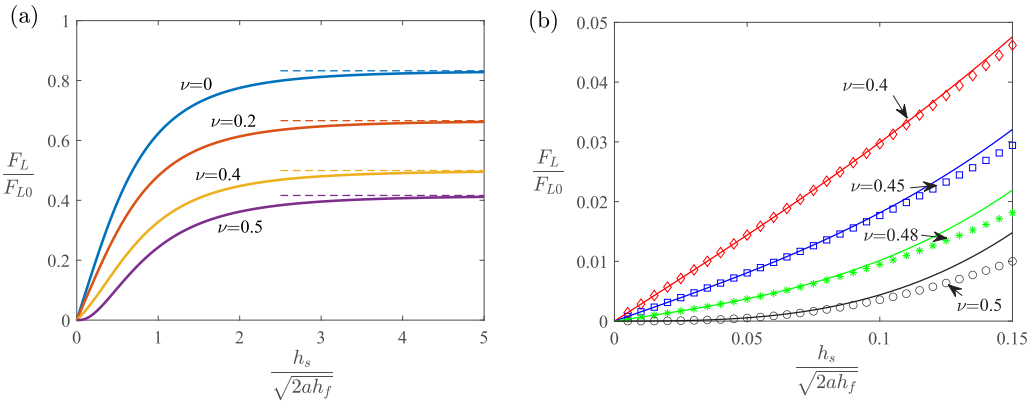

FIG. 2. (a) Normalized lift force versus normalized layer's depth for various Poisson's ratios; $F_{L0} = \eta^2 {v_p}^2 a^{\frac{5}{2}}/(\mu {h_f}^{\frac{5}{2}})$. The dashed lines show the thick-layer approximation given by Eq. (26). (b) Normalized lift force versus normalized thickness for thin layers. The markers represent the exact result obtained from Eq. (26) while the solid lines show the small-H_s approximation Eq. (27), retaining up to cubic terms.

perturbation of the elastohydrodynamic Reynolds lubrication equation. Taylor expansion of the general expression Eq. (26) for large H_s shows that the next term is $O[(\log H_s)^2 H_s^{-5}]$. The curves converge relatively quickly to their $H_s \to \infty$ limits, as shown in Fig. 2(a). The infinitely-thick-layer asymptote is accurate to within 0.2% at $H_s = 5$ and within 10% with $H_s = 2.25$ for the case of $\nu = 0.5$. For other values of Poisson's ratio, the error is of the same order of magnitude.

For thin layers ($H_s \ll 1$), we Taylor expand Eq. (26) about $H_s = 0$ and evaluate the integral. By extracting the first three terms, we obtain the following asymptotic behavior

$$F_L = \frac{\eta^2 {v_p}^2 a^{\frac{5}{2}}}{\mu\, {h_f}^{\frac{5}{2}}} \frac{24\sqrt{2}\pi}{125} \left[\frac{1-2\nu}{1-\nu} H_s + \frac{18\nu(4\nu-1)}{7(1-\nu)^2} {H_s}^3 - \frac{64(3-30\nu+76\nu^2+16\nu^3)}{35(1-\nu)^3} H_s^5 + O\big(H_s^7\big) \right]. \tag{27}$$

As depicted in Fig. 2(b), the two-term Taylor series expansion represents the exact result with good accuracy for $H_s \lesssim 0.1$ for ν close to 0.5 although the range of accuracy of the expansion is extended for smaller values of ν. Including terms of $O(H_s^5)$ and higher yields only a slight improvement in accuracy. For $H_s \ll 1$, the linear term dominates for almost all values of ν. Writing ν in this equation in terms of Lamé's constants (μ and λ) and retaining just the $O(H_s)$ term leads to $F_L = (48\sqrt{2}\pi\ \eta^2 {v_p}^2 a^{\frac{5}{2}} H_\ell)/(125(2\mu+\lambda){h_f}^{\frac{5}{2}})$, in agreement with the result of Urzay *et al.* [15], obtained using a Winkler model for the solid. Thus, the limiting values of forces for both thin [15] and thick [29] layers are obtained within a single consistent formalism.

While the Winkler model typically produces a good approximation of the force for thin layers, it admits no deformation and therefore no lift force for a strictly incompressible solid. As shown by Eq. (27), at $\nu = 1/2$ representing a perfectly incompressible solid, the term linear in H_s vanishes and leaves behind $F_L \propto {H_s}^3$. This cubic scaling of the force is a signature of an incompressible response of the material [14]. However, in practice, soft materials are only approximately incompressible, so it relevant to quantify the crossover between compressible ($F_L \propto H_s$) and incompressible ($F_L \propto {H_s}^3$) behaviors to assess the relative importance of each. This crossover is shown in Fig. 3: for small values of H_s, the linear scaling is observed except for the degenerate case of $\nu = 1/2$, where the leading term scales as H_s^3. As one may observe in Fig. 3, for each Poisson's ratio, there is a characteristic thickness across which the cubic and linear terms intersect. By comparing the first

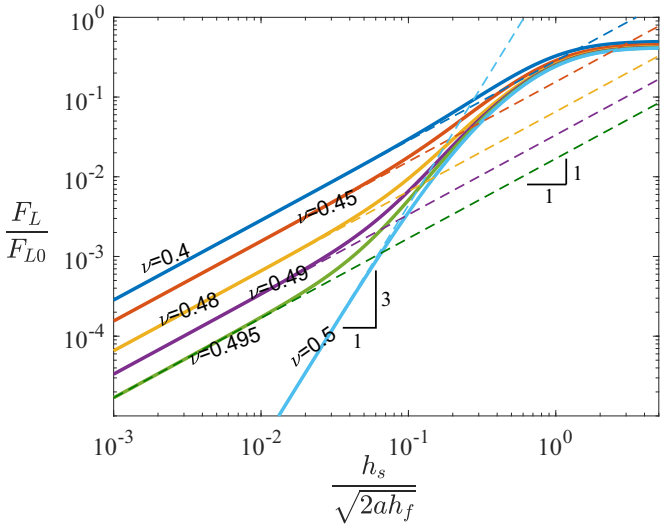

FIG. 3. The normalized lift force versus normalized thickness for different Poisson's ratios. $F_{L0} = \eta^2 {v_p}^2 a^{\frac{5}{2}} / (\mu {h_f}^{\frac{5}{2}})$. The solid lines are results from the full theory, while dashed lines are leading-order approximations for small thickness.

two terms in Eq. (27), this crossover thickness is found to be $H_s^c = \sqrt{\frac{7}{18}} \frac{\sqrt{2\nu^2-3\nu+1}}{\sqrt{4\nu^2-\nu}}$ which, for ν close to $1/2$, behaves as $H_s^c \sim \sqrt{7/9}(1/2-\nu)^{1/2}$.

This behavior is understood by recognizing there are two separate modes of deformation of the elastic layer: compression and shear. For a thin layer, these two effects scale differently with the layer thickness H_s: In Eq. (27), the linear term represents the compression mechanism and the cubic term represents the shear. For thin compressible materials, compression dominates for small H_s. In fully incompressible materials ($\nu = 1/2$), however, shear is the only mode of deformation. Thus, for nearly incompressible materials ($1/2 - \nu \ll 1$), compressive effects are weak and compete with shear when $H_s \simeq (1/2-\nu)^{1/2}$ (see Ref. [36] for a detailed discussion).

From this simple estimate, one may expect the linear scaling to hold when $H_s \ll H_s^c$; this is indeed the case as evidenced by Fig. 3. Contrarily, one might expect the incompressible scaling to become relevant if $H_s \gg H_s^c$, provided that the layer is still thin. While this is true, the small-thickness asymptotics are found to be ineffective as an approximation for Eq. (25) for layers thicker than $H_s \gtrsim 0.12$ for $\nu \simeq 1/2$ (cf. Fig. 3). Thus, any H_s^3 scaling behavior of the force would only be observable only in a very narrow range of H_s given by

$$\frac{\sqrt{7}}{3}\left(\frac{1}{2}-\nu\right)^{1/2} \ll H_s \lesssim 0.12. \tag{28}$$

For $\nu = 0.495$, the lower bound is about 0.063 so even for this "nearly incompressible" value of ν, the condition Eq. (28) is extremely restrictive. Indeed, as can be seen in Fig. 3, the incompressible scaling $F_L \propto H_s^3$ is not observable even with ν as large as 0.495. For $\nu = 0.499$ (not plotted) there is an barely identifiable range of H_s where $F_L \propto H_s^3$. These behaviors may be rationalized from the Green's function for the elastic layer (see [10]), albeit modulated here via the integral Eq. (25). This is consistent with the results of Chandler and Vella [36] for cylindrical contacts (see also the Appendix).

To summarize, even when ν is very near to 0.5, the Winkler model accurately predicts the force ($F_L \propto H_s$) for a thin enough layer ($H_s \lesssim H_s^c \approx \sqrt{1/2-\nu}$). Up to $\nu \approx 0.495$, the Winkler approximation holds when $H_s \lesssim 0.1$. For each $\nu \lesssim 1/2$ and for $H_s \gtrsim \sqrt{1/2-\nu}$, there is a transition region

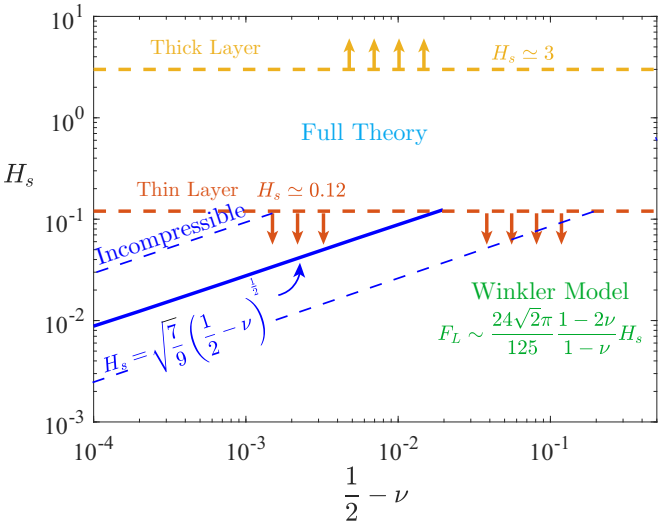

FIG. 4. Phase diagram on the H_s-ν plane indicating the qualitative behavior of the lift force in different regions. The thin-layer approximation for the force Eq. (27) is typically applicable for $H \lesssim 0.12$. The incompressible scaling $F_L \propto H_s^3$ is only realized in a narrow range of Poisson ratio $1/2 \leqslant \nu < 0.495$ with $(1/2-\nu)^{1/2} \ll H_s \ll 0.12$. The Winkler approximation is effective for $H \ll (1/2-\nu)^{1/2}$ for ν close to $1/2$. The thick layer approximation is accurate for $H \gtrsim 3$.

where the behavior of F_L is a combination of linear and cubic powers of H_s. Beyond this region ($H_s \gg \sqrt{1/2-\nu}$) the layer may behave like a fully incompressible solid in principle although this behavior is quickly suppressed by higher order terms for $H_s \gtrsim 0.12$. Thus, the incompressible $F_L \propto H_s^3$ scaling is only applicable in a limited range of Poisson's ratio $0.495 \lesssim \nu \leqslant 1/2$ over a limited range of layer thickness $\sqrt{1/2-\nu} \ll H_s \lesssim 0.12$; this is far more restrictive is suggested by the value of the Poisson ratio's alone. The thin-layer approximations appear valid for $H \lesssim 0.12$ for ν close to $1/2$. Beyond this value, the full integral Eq. (25) is necessary to obtain a quantitatively accurate prediction. We summarize the different lift force approximations and their regions of validity in Fig. 4. This serves as a qualitative guide to choose an approximation for the force based on the normalized layer's thickness H_s and Poisson's ratio ν.

The above results for thin and thick layers are in agreement with the available experimental results in the literature. The result Eq. (26) agrees with the data of Ref. [29], which measure the force on a sphere translating past a thick elastic layer ($H_s \gg 1$). For thin layers, our results for a cylinder [see Appendix, Eq. (A8)] nearby a nearly incompressible layer ($\nu \sim 0.49$) are in good agreement with the experiments of Ref. [28] for small to intermediate values of H_s.

B. Oscillatory excitation and the effects of viscoelasticity

The results of the previous section assumed that the behavior of the fluid and the solid are both time-independent. However, this may not always be the case in experiments. Recent experimental work by Ref. [29] drove tangential oscillations of sphere (attached to an atomic force microscope tip) next to a thick elastomeric layer and measured the cycle-average lift force on the sphere resulting from this oscillatory driving. In these particular experiments, the measured average lift force was found to be consistent with a strictly elastic model of the substrate. However, it may be important to account for a finite relaxation time of the solid response for more general soft materials, particularly when the oscillation frequency is close to an inverse relaxation timescale of the material. In the following, we apply the framework developed here to oscillatory motion, accounting for a

general linear viscoelastic response of the solid. As we show below, the measured lift force contains contributions from both the storage and loss moduli of the substrate.

We focus on the situation in which the sphere oscillates with a small amplitude at a single frequency ω with a peak speed v_{p0} along the x direction. We set the origin of time t such that the position and velocity of the sphere are

$$x_p(t) = \frac{v_{p0}}{\omega_0} \sin \omega_0 t, \tag{29a}$$

$$v_p(t) = v_{p0} \cos \omega_0 t = v_{p0}\, \mathrm{Re}_j\{\exp(j\omega_0 t)\}. \tag{29b}$$

Note that j is the imaginary unit in the complex time space (Re_j identifies the real part of a function in the j complex plane) and is distinct from the imaginary unit i used to characterize spatial Fourier modes in the foregoing analysis. We will neglect inertial effects as before, although we note that oscillatory inertia may produce additional forces. Neglecting transients from the start-up of the motion, the (leading-order) pressure and velocity fields are also harmonic,

$$p(\mathbf{x}, t) = p_0(\mathbf{x})\, \mathrm{Re}_j\{\exp(j\omega_0 t)\}, \quad \mathbf{v}(\mathbf{x}, t) = \mathbf{v}_0(\mathbf{x})\, \mathrm{Re}_j\{\exp(j\omega_0 t)\}, \tag{30}$$

up to correction terms of $O(\Lambda)$. It is important to note that p and $\mathbf{v}$ are in phase with v_p since the leading-order pressure is governed by the (quasistatic) Stokes equations with rigid boundaries (i.e., $p_0(\mathbf{x})$ and $\mathbf{v}_0(\mathbf{x})$ are real functions with respect to j).

Assuming that the oscillating leading-order pressure elicits a linear response as before, we can write the spatially Fourier transformed surface displacement of the substrate as

$$\tilde{\delta}(\mathbf{q}', t) = \mathrm{Re}_j\{-\tilde{p}_0(\mathbf{q}')\tilde{G}(\mathbf{q}', \omega_0)\, \exp(j\omega_0 t)\}. \tag{31}$$

Here, $G(\mathbf{x}, \omega_0)$ is the complex (in the j plane) oscillatory viscoelastic response function of the material (corresponding to an oscillating normal point force) and $\tilde{G}(\mathbf{q}', \omega_0)$ is its spatial Fourier transform. Equation (31) is the dimensional equivalent of Eq. (19) for oscillatory forcing.

We now introduce the dimensionless frequency parameter $\omega = \omega_0 \ell / v_{p0}$ and rescale variables as before, using v_{p0} and $\eta v_{p0} \ell / h_f^2$ to scale velocities and pressure in the main problem. The solution to the model problem is unchanged from before, and still corresponds to the steady motion of a sphere away from a rigid wall. The flow fields of the main problem under oscillatory driving are formed by modulating their steady counterparts with a temporal oscillation, making use of the fact that the leading-order flow oscillates in phase with the particle. For example, the pressure in the main problem is $P(R, \theta) \cos \omega T$; similarly, the velocity field is a $\cos \omega T$ modulated version of Eqs. (14b) and (14c). In general, the effective shear modulus of a viscoelastic material is frequency dependent, so we introduce the zero-frequency shear modulus scale μ_0 and use it to define the dimensionless complex response function $\mathcal{G} = 2|\mu_0|\ell G$ and its spatial Fourier transform $\tilde{\mathcal{G}} = 2|\mu_0|\tilde{G}/\ell$. In dimensionless variables, $\tilde{\Delta}(\mathbf{q}, T) = \mathrm{Re}_j\{-\tilde{P}(\mathbf{q})\tilde{\mathcal{G}}(\mathbf{q}, \omega)\, \exp(j\omega T)\}$.

To analyze the lift force, we start with Eq. (17), but with v_p replaced by v_{p0}, which is valid for time-dependent motion. We follow the same steps as before and recast Eq. (17) as an integral over the dimensionless Fourier variable $\mathbf{q}$. We now retain the time-derivative term in Eq. (17) and keep track of the time-dependence explicitly to obtain the analog to Eq. (21a),

$$\begin{aligned} F_L = \frac{\eta^2 {v_{p0}}^2 \ell^5}{8\pi^2 |\mu_0|\, {h_f}^5} \Bigg(& \int_0^{2\pi} \int_0^{\infty} \mathrm{Re}_j\left\{ j\omega \tilde{\tilde{P}} \tilde{P}^* [\tilde{\mathcal{G}}(\mathbf{q}, \omega_0)]^* \exp(j\omega T) \right\} \Big|_{Z=0} q\, dq\, d\varphi \\ & + \int_0^{2\pi} \int_0^{\infty} \mathrm{Re}_j \Bigg[\left(i\tilde{\tilde{P}} q \cos\varphi + \widetilde{\frac{\partial \hat{V}_r}{\partial Z} \frac{\partial V_r}{\partial Z}} \right) \\ & \times \cos(\omega T)\, \tilde{P}^* \{\tilde{\mathcal{G}}(\mathbf{q}, \omega_0)\}^* \exp(j\omega T) \Bigg] \Bigg|_{Z=0} q\, dq\, d\varphi \Bigg), \end{aligned} \tag{32}$$

where the asterisk denotes the complex conjugate in the i plane as before. The first integral term results from the time-derivative of the deformation field in Eq. (17), while the second integral is the same as in Eq. (21a) except for the time dependences, with the $\cos(\omega T)$ being contributed by the main-problem fields in Eq. (17) and the complex exponential being contributed by $\tilde{\Delta}$, cf. Eq. (31).

The complex response $\tilde{\mathcal{G}}$ is written in terms of its real and imaginary parts as

$$\tilde{\mathcal{G}}(\mathbf{q},\omega) = \tilde{\mathcal{G}}'(\mathbf{q},\omega) + j\tilde{\mathcal{G}}''(\mathbf{q},\omega), \tag{33}$$

where $\tilde{\mathcal{G}}'$ and $\tilde{\mathcal{G}}''$ are, respectively, spatial Fourier transforms of the storage and loss responses of the material. Note that the $\tilde{\mathcal{G}}$ characterizes the elastic deformation, so $\tilde{\mathcal{G}}'$ and $\tilde{\mathcal{G}}''$ are related to the real and imaginary parts, respectively of the (frequency-dependent) reciprocal complex shear modulus $1/\mu(\omega)$. The Poisson's ratio may also be frequency-dependent in principle, although we neglect this dependence here. Substituting the results Eq. (22) into Eq. (32) and simplifying leads to

$$\begin{aligned} F_L = \frac{9\,\eta^2 {v_p}^2 a^{\frac{5}{2}}}{25\sqrt{2}\,|\mu_0|\,{h_f}^{\frac{5}{2}}} \int_0^\infty \int_0^{2\pi} \Big\{ & 5i\omega\, q^3 K_0(q) K_1(q) \big[\tilde{\mathcal{G}}'(\mathbf{q},\omega)\sin(\omega T) + \tilde{\mathcal{G}}''(\mathbf{q},\omega)\cos(\omega T)\big]^* \cos\varphi \\ & + \frac{1}{2} q^5 [K_0(q)]^2 \big[\tilde{\mathcal{G}}'(\mathbf{q},\omega)\big]^* \cos^2\varphi + \frac{1}{2} q^5 [K_0(q)]^2 \big[\tilde{\mathcal{G}}'(\mathbf{q},\omega)\cos(2\omega T) \\ & - \tilde{\mathcal{G}}''(\mathbf{q},\omega)\sin(2\omega T)\big]^* \cos^2\varphi \Big\}\, d\varphi\, dq. \end{aligned} \tag{34}$$

The above result yields the lift force at linear order in Λ for oscillatory translation of a sphere parallel to a linear viscoelastic substrate, and is the oscillatory analog of (23). Note that setting $\omega = 0$ above recovers the steady-state result. Note again that the above result applies to any substrate whose deformation is linearly related to the applied normal stresses through a Green's function $\tilde{G}(\mathbf{q},\omega)$.

In general, the lift force comprises a superposition of a steady component, contributions oscillating at the driving frequency ω and contributions oscillating at 2ω. The mean force over an oscillation cycle is

$$\langle F_L \rangle = \frac{9\,\eta^2 {v_p}^2 a^{\frac{5}{2}}}{25\sqrt{2}\,|\mu_0|\,{h_f}^{\frac{5}{2}}} \int_0^\infty \int_0^{2\pi} \frac{1}{2} q^5 \{K_0(q)\}^2 \big\{\tilde{\mathcal{G}}'(\mathbf{q},\omega)\big\}^* \cos^2\varphi\, d\varphi\, dq. \tag{35}$$

Note the similarity with Eq. (23), except for a factor of $1/2$ arising from the averaging over the cycle. Thus, the mean lift force corresponds to using the elastic (storage) response of the material $\tilde{\mathcal{G}}'$ at the driving frequency, utilizing the steady-state result Eq. (23) quasi-statically at each point in the oscillation cycle, and then averaging over the oscillation cycle. Indeed, this quasi-static assumption was employed by Ref. [29] for a strictly elastic model; Eq. (35) shows that this approach is also valid for a viscoelastic response irrespective of the relaxation timescale of the solid relative to the driving frequency.

While the mean lift force only depends on the storage response $\tilde{\mathcal{G}}'$, oscillating components of the force depend on both the storage and loss response functions. Terms oscillating at frequency ω are only nonzero if the response of the solid has an asymmetric component in the direction of translation (caused, for example, by a gradient of mechanical properties). Thus, for most typical materials with symmetric stress responses, a force component at frequency ω is not expected to be generated. The contribution to the force oscillating with twice the driving frequency is

$$\begin{aligned} F_L^{(2\omega)} = \frac{9\,\eta^2 {v_{p0}}^2 a^{\frac{5}{2}}}{25\sqrt{2}\,|\mu_0|\,{h_f}^{\frac{5}{2}}} \int_0^\infty \int_0^{2\pi} \frac{1}{2} q^5 \{K_0(q)\}^2 \{\tilde{\mathcal{G}}'(\mathbf{q},\omega)\cos(2\omega T) \\ - \tilde{\mathcal{G}}''(\mathbf{q},\omega)\sin(2\omega T)\}^* \cos^2\varphi\, d\varphi\, dq. \end{aligned} \tag{36}$$

The part of this force component that oscillates as $\cos(2\omega T)$ is in phase with ${v_p(t)}^2 \propto \cos^2(\omega T)$ and depends on the storage response $\tilde{\mathcal{G}}'$, whereas the component oscillating as $\sin(2\omega T)$ is 90

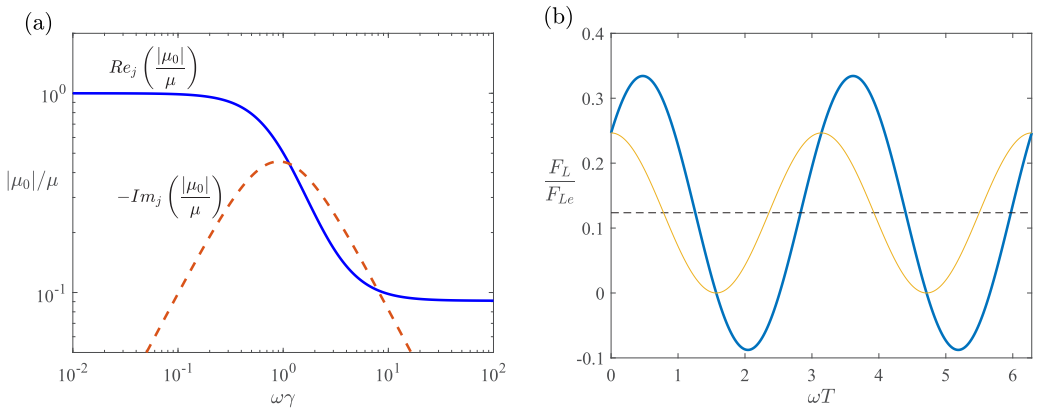

FIG. 5. (a) The real and imaginary part of normalized reciprocal complex modulus for standard linear solid model. (b) Rescaled viscoelastic lift force (thick curve) F_L/F_{Le} over one period; $F_{Le} = 243\,\pi^3\eta^2 {v_{p0}}^2\, a^{\frac{5}{2}}(1-\nu)/(|\mu_0|\, {h_f}^{\frac{5}{2}}\, 6400\sqrt{2})$ is the zero-frequency limit of Eq. (37). The dashed line indicates the mean over the cycle and the thin curve is the elastic part of the response, in phase with $v_p(t)^2$. We use $c = 10$ in both plots and $\omega\gamma = 2$ in (b).

degrees out of phase with $v_p(t)^2$ and depends on the loss response $\tilde{\mathcal{G}}''$. Thus, amplitude and phase information of the 2ω frequency component of F_L can be used to infer the complex viscoelastic modulus of the substrate.

As a concrete example, we apply the result Eq. (36) to a viscoelastic layer. For simplicity, we focus on the limit of a thick layer and consider the shear modulus to be a complex frequency-dependent function $\mu(\omega)$ as is typical in linear viscoelasticity. Then, the time-dependent lift force for oscillatory forcing in this case is

$$F_L = \frac{\eta^2 {v_{p0}}^2\, a^{\frac{5}{2}}}{|\mu_0|\, {h_f}^{\frac{5}{2}}}\,\frac{243\,\pi^3(1-\nu)}{12800\sqrt{2}}\left\{\mathrm{Re}_j\left[\frac{|\mu_0|}{\mu(\omega)}\right] + \mathrm{Re}_j\left[\frac{|\mu_0|}{\mu(\omega)}\right]\cos(2\omega T) - \mathrm{Im}_j\left[\frac{|\mu_0|}{\mu(\omega)}\right]\sin(2\omega T)\right\}, \tag{37}$$

where we have assumed that ν is frequency-independent and $\mu_0 = \mu(\omega = 0)$ is the zero-frequency shear modulus by definition. Note that the lift force does not contain terms at frequency ω due to the isotropy of the response function. From Eq. (37), we find that the amplitude of the oscillating component of the force exceeds the magnitude of the mean force by a multiplicative factor $\{1 + (\mathrm{Im}_j\{\mu\}/\mathrm{Re}_j\{\mu\})^2\}^{1/2}$. Thus, a positive lift force throughout the oscillation cycle indicates a purely elastic response, whereas a negative lift force (i.e., attraction) during a part of the cycle signals a viscous response from the material. Note that the mean lift force is always positive.

To illustrate these predictions, we evaluate Eq. (37) for a specific rheological model of the substrate. A simple and practically relevant viscoelastic model for soft solids is the standard linear solid (SLS; or Zener) model. This model represents the resistance of the solid by a spring and damper in parallel, connected in series to another spring. The complex shear modulus for this model is (see Ref. [17])

$$\frac{\mu(\omega)}{|\mu_0|} = \frac{(\omega\gamma)^2 + c^2 + c(\omega\gamma)^2}{(\omega\gamma)^2 + c^2} + j\,\frac{c^2(\omega\gamma)}{(\omega\gamma)^2 + c^2}, \tag{38}$$

where c is the ratio between the two spring stiffnesses in the model (see Ref. [17] for more details) and $\gamma = \tau_s v_{p0}/\ell$ is the ratio of viscoelastic relaxation time constant τ_s of the material to the time scale of advection. We utilize this model to evaluate the real and imaginary parts of normalized reciprocal complex modulus [Fig. 5(a)] and the total lift force described by Eq. (37)

for a specific value of stiffness ratio $c = 10$. As shown in Fig. 5(b) at a frequency $\omega\gamma = 2$, the rescaled force F_L/F_{Le} oscillates about a mean of $\frac{1}{2}\mathrm{Re}_j\{\mu_0/\mu(\omega)\}$ with frequency 2ω, where F_{Le} is the zero-frequency limit of Eq. (37). The amplitude of force oscillations exceeds the mean force, which is a signature of a viscoelastic material response.

The general result Eq. (34) and its more specific application Eq. (37) suggest opportunities for noncontact microrheometry of soft materials through lift force measurements. Isolating and analyzing the different temporal frequency components of the $F_L(t)$ response can provide insights into the frequency-dependent viscoelastic material response. For example, it is expected that an experiment such as that of Zhang *et al.* [29] with an oscillatory driving yields a measurable time-dependent lift force $F_L(t)$. At any given driving frequency ω, the components of $F_L(t)$ in phase with $\cos(2\omega T)$ and $\sin(2\omega T)$ yield the real and imaginary parts of $1/\mu(\omega)$, respectively, as given by Eq. (37). Thus, repeating this experiment at different frequencies ω would enable a reconstruction of the complex modulus $\mu(\omega)$ over a range of frequencies, thus characterizing the visoelastic material response. Equation (34) [Eq. (23) for the steady case] may also be useful to characterize the spatial frequency spectrum of a soft material with an unknown response function $\tilde{\mathcal{G}}(\mathbf{q}, \omega)$. We note that the material response is probed on the characteristic length scale $\ell = \sqrt{2ah_f}$ set by the lubrication geometry, ultimately leading to the lift force. Measuring F_L at different gap widths h_f (other geometric and physical parameters kept constant), Eq. (23) yields a set of integral equations relating F_L and the (unknown) response function $\tilde{\mathcal{G}}(\mathbf{q})$, where we drop the ω dependence for clarity. Solving these relations for $\tilde{\mathcal{G}}(\mathbf{q})$ may provide insights into the material response at spatial frequencies $|\mathbf{q}| \sim \ell^{-1} = (2ah_f)^{-1/2}$. We note, however, that the robustness of inverting the integral relations Eq. (34) subject to experimental uncertainties is nontrivial and warrants a more careful study.

Finally, we remark that although the calculation in this section has focused on harmonic driving, the result Eq. (17) is general and, with a combination of spatial and temporal transforms, can be used to calculate the lift force in more general time dependent situations. Such a calculation would, in general, involve an integral over all temporal frequency components and is not detailed here; see Ref. [17] for a detailed analysis of the start-up of motion using the direct perturbation solution of the Reynolds equation.

V. CONCLUSIONS

We have introduced a general theoretical framework to calculate the lift force on a locally spherical surface moving parallel to soft substrate separated by a lubricating liquid film. The application of the Lorentz reciprocal theorem and a transformation to Fourier space yields a compact relation between the lift force and the linear response function (i.e., the Green's function) of the substrate. The upshot of this formalism is that it applies to an arbitrary soft material that exhibits a linear stress-displacement response for small applied stresses.

Applying this general formulation to a linearly elastic layer of finite thickness, we studied the behavior of lift force as a function of the thickness and Poisson's ratio of the layer. Our results reveal a compact analytic result for all layer thicknesses and material compressibilities, while recovering the results of previous experimental and theoretical work for thick and thin elastic layers. For thin layers, we find a transition of the force between the results of a Winkler model dominated by compression and incompressible thin-layer theory dominated by internal shearing of the material.

Finally, we generalized the theory for linear elastic materials to linear viscoelastic materials. For oscillatory relative motion between the surfaces, we obtain a time-dependent lift force and find that different temporal Fourier components of the force are controlled by either the elastic or viscous parts of the substrate response. For steady and time-periodic motion, the framework developed here yields the general results Eqs. (23) and (34), respectively, for the lift force.

Thus, the framework provides a powerful and versatile tool to directly compute lift forces in situations involving elastohydrodynamic lubrication. We anticipate that the methods developed here and the specific results will be useful to characterize forces on objects interacting with soft

materials and deformable interfaces at the microscale. The formalism may also provide insights into the mechanical properties of soft materials via measurements of lift forces in contactless micro-rheometry experiments at different frequencies and gap widths. Understanding the robustness of such an approach to experimental uncertainties requires a detailed study and is a potential topic for future research.

ACKNOWLEDGMENT

The authors are grateful to Dr. Thomas Salez for helpful discussions. A.K.-E. acknowledges support from the Dean's Distinguished Fellowship Award of the University of California, Riverside.

APPENDIX: LIFT FORCE ON A CYLINDER MOVING PARALLEL TO A SOFT SUBSTRATE

Here, we employ the approach of the main text to find the lift force on a cylinder moving parallel to a nearby soft wall. While the direct perturbation approach is more analytically tractable for cylinders, at least for a thin or thick elastic layers, the formulation here offers a convenient route to the lift force for general material responses. The formulation for a cylinder, starting with Eq. (9), is similar as before and requires solutions to the main and model problems. In the model problem, a cylinder moves normal to a rigid wall ($\hat{\mathbf{v}}_p = \hat{v}_p\,\mathbf{e}_z$). Again, Eq. (10) can be employed to normalize the relations except that R is replaced by $X = x/\ell$. The relevant results for the model problem are

$$\hat{P} = -\frac{3}{(1+X^2)^2}, \tag{A1a}$$

$$\left.\frac{\partial \hat{V}_x}{\partial Z}\right|_{Z=0} = -\frac{6X}{(1+X^2)^2}. \tag{A1b}$$

The main problem describes the motion of a cylinder with the velocity $\mathbf{v}_p = v_p\,\mathbf{e}_x$. After normalization as in Eq. (13), one finds

$$P = \frac{2X}{(1+X^2)^2}, \tag{A2a}$$

$$\left.\frac{\partial V_x}{\partial Z}\right|_{Z=0} = \frac{4X^2}{(1+X^2)^2}. \tag{A2b}$$

Both main and model problems are well-known in the literature (see, e.g., [14]). After substituting the relevant results into Eq. (9) and we obtain the lift force per length of the cylinder

$$F_L = -\frac{\eta^2 {v_p}^2\,\ell^4}{2\mu\,{h_f}^5}\int_{-\infty}^{\infty}\left[\hat{P}\frac{\partial\Delta}{\partial T} - \hat{P}\left(\frac{\partial\Delta}{\partial X}\right) + \Delta\frac{\partial\hat{V}_x}{\partial Z}\frac{\partial V_x}{\partial Z}\right]\Bigg|_{Z=0} dX. \tag{A3}$$

We introduce a one-dimensional dimensionless Fourier variable $q_x \in (-\infty, \infty)$ dual to X. Note that this is related to the polar Fourier variable introduced in the main text as $q_x = q\cos\varphi$. Parseval's theorem lets us cast Eq. (A3) as an integral in Fourier space. At steady state,

$$F_L = \frac{2\eta^2 {v_p}^2 a^2}{\mu {h_f}^3}\int_{-\infty}^{\infty}\left(iq\tilde{\tilde{P}} + \widetilde{\frac{\partial\hat{V}_x}{\partial Z}\frac{\partial V_x}{\partial Z}}\right)\left(\tilde{\mathcal{G}}\,\tilde{P}\right)^*\Bigg|_{Z=0}\frac{dq_x}{2\pi}. \tag{A4}$$

Here, $\tilde{\mathcal{G}}(q_x)$ is the transformed response function and yields the transformed displacement via $\tilde{\Delta}(q_x) = \tilde{G}(q_x)\tilde{P}(q_x)$. Evaluating the Fourier transforms of the result Eqs. (A1) and (A2) and substituting them into Eq. (A4) yields the general steady-state result for a cylinder

$$F_L = \frac{\pi\,\eta^2 {v_p}^2\,a^2}{2\mu\,{h_f}^3}\int_{-\infty}^{\infty} e^{-2|q_x|}\,{q_x}^4\,\tilde{\mathcal{G}}^*(q_x)\,dq_x. \tag{A5}$$

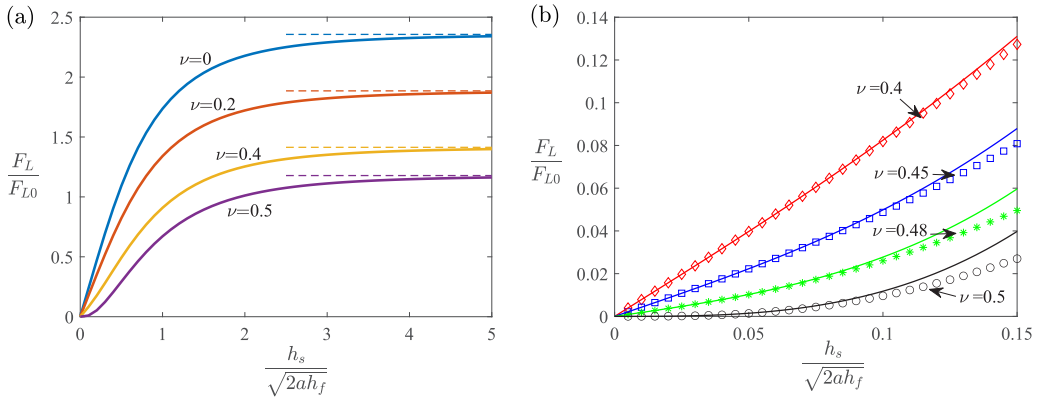

FIG. 6. (a) Normalized lift force versus normalized layer's depth for various Poisson's ratios; $F_{L0} = \eta^2 {v_p}^2 a^2/(\mu {h_f}^3)$ is the characteristic scale of the lift force per length. the dashed lines show the infinity approximation by Eq. (A7). (b) Normalized lift force versus normalized thickness for thin layers limit. The markers represent the main function while the solid lines show the thin-layer approximation up to terms of $O(H_s^3)$.

For an elastic layer, the transformed Green's function $\tilde{\mathcal{G}}$ is obtained from Eq. (24) with some minor modifications involving the change from polar to one-dimensional Cartesian geometry. In particular, noting that the polar Fourier variable $q = \sqrt{{q_x}^2 + {q_y}^2}$ and setting $q_y = 0$ (because the cylinder problem is two-dimensional), the Green's function relevant to the cylinder problem corresponds to a solid layer with line loading and is given by

$$\tilde{\mathcal{G}}(q_x) = \frac{2(1-\nu)}{|q_x|}\left[\frac{(3-4\nu)\ \sinh(2|q_x|H_s) - 2|q_x|H_s}{(3-4\nu)\ \cosh(2|q_x|H_s) + 2(|q_x|H_s)^2 + 5 - 12\nu + 8\nu^2}\right], \tag{A6}$$

where $|q_x|$ is the absolute value of the one-dimensional Fourier parameter.

Substituting Eqs. (A6) into (A5) and integrating yields the lift force on a cylinder for a layer with an arbitrary thickness and Poisson's ratio. In Fig. 6(a), the force is plotted for several values of these two parameters. The results for the cylinder are qualitatively similar to those for the sphere, with only some minor quantitative differences.

In the case of an infinitely thick layer, the lift force reduces to

$$F_L(H_s \to \infty) = \frac{\eta^2 {v_p}^2 a^2}{\mu\, {h_f}^3}\ \frac{3\pi(1-\nu)}{4}, \tag{A7}$$

in agreement with Ref. [14]. As one can observe in Fig. 6(a), the lift force converges to the infinite-thickness limit relatively quickly and a layer with the thickness of $H_s = 5\sqrt{h_f a}$ could be considered effectively infinite with good accuracy. In the thin-layers regime ($H_s \ll 1$), using Taylor's series expansion of $\tilde{\mathcal{G}}$, we lift force has the asymptotic behavior

$$F_L = \frac{\eta^2 {v_p}^2 a^2}{\mu\, {h_f}^3}\frac{3\pi}{4}\left[\frac{1-2\nu}{1-\nu}H_s + \frac{5\nu(4\nu-1)}{2(1-\nu)^2}{H_s}^3 + O\big({H_s}^5\big)\right]. \tag{A8}$$

The linear term in Eq. (A8) reproduces the result of using the Winkler approximation [13]. Figure 6(b) compares the behavior of Taylor series expansion (A8) and the main function. As with the sphere, for $H_s < 0.1$, the approximation describes the exact result with good accuracy. The transition between compressible and incompressible scaling behaviors is depicted in Fig. 7 (compare with Fig. 3). For the cylinder, the crossover thickness is found to be $H_c = \frac{\sqrt{\frac{2}{5}}\sqrt{2\nu^2-3\nu+1}}{\sqrt{4\nu^2-\nu}} \sim \sqrt{4/5}\,(1/2-\nu)^{1/2}$ (see also Ref. [36]). As with the sphere, the Winkler model provides a good

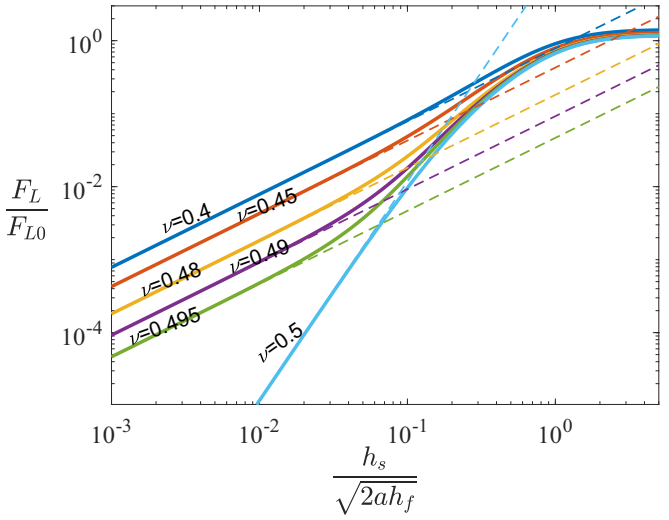

FIG. 7. The normalized lift force versus normalized thickness for different Poisson's ratios. Here, $F_{L0} = \eta^2 {v_p}^2 a^2/(\mu {h_f}^3)$ is the characteristic scale of the lift force per length. The solid lines are the exact results while the dashed lines are one-term approximations for thin layers.

representation of the force for thin layers except in an extremely narrow range of H_s for materials with $1/2 - \nu \lesssim 10^{-3}$.

[1] B. J. Hamrock, S. R. Schmid, and B. O. Jacobson, *Fundamentals of Fluid Film Lubrication* (CRC Press, Boca Raton, 2004).

[2] V. C. Mow, M. H. Holmes, and W. M. Lai, Fluid transport and mechanical properties of articular cartilage: A review, J. Biomech. **17**, 377 (1984).

[3] C. S. Campbell, Self-lubrication for long runout landslides, J. Geol. **97**, 653 (1989).

[4] K. Sekimoto and L. Leibler, A mechanism for shear thickening of polymer-bearing surfaces: Elasto-hydrodynamic coupling, Europhys. Lett. **23**, 113 (1993).

[5] J. B. Freund, Numerical simulation of flowing blood cells, Annu. Rev. Fluid Mech. **46**, 67 (2014).

[6] M. Abkarian, C. Lartigue, and A. Viallat, Tank Treading and Unbinding of Deformable Vesicles in Shear Flow: Determination of the Lift Force, Phys. Rev. Lett. **88**, 068103 (2002).

[7] R. H. Davis, J.-M. Serayssol, and E. J. Hinch, The elastohydrodynamic collision of two spheres, J. Fluid Mech. **163**, 479 (1986).

[8] A. Bizzarri, The mechanics of lubricated faults: Insights from 3D numerical models, J. Geophys. Res. **117**, B05304 (2012).

[9] D. Wirtz, Particle-tracking microrheology of living cells: Principles and applications, Annu. Rev. Biophys. **38**, 301 (2009).

[10] S. Leroy and E. Charlaix, Hydrodynamic interactions for the measurement of thin film elastic properties, J. Fluid Mech. **674**, 389 (2011).

[11] Y. Wang, M. R. Tan, and J. Frechette, Elastic deformation of soft coatings due to lubrication forces, Soft Matter **13**, 6718 (2017).

[12] M. E. O'neill and K. Stewartson, On the slow motion of a sphere parallel to a nearby plane wall, J. Fluid Mech. **27**, 705 (1967).

[13] J. M. Skotheim and L. Mahadevan, Soft Lubrication, Phys. Rev. Lett. **92**, 245509 (2004).

[14] J. M. Skotheim and L. Mahadevan, Soft lubrication: The elastohydrodynamics of nonconforming and conforming contacts, Phys. Fluids **17**, 092101 (2005).
[15] J. Urzay, S. G. Llewellyn Smith, and B. J. Glover, The elastohydrodynamic force on a sphere near a soft wall, Phys. Fluids **19**, 103106 (2007).
[16] N. J. Balmforth, C. J. Cawthorn, and R. V. Craster, Contact in a viscous fluid. Part 2. A compressible fluid and an elastic solid, J. Fluid Mech. **646**, 339 (2010).
[17] A. Pandey, S. Karpitschka, C. H. Venner, and J. H. Snoeijer, Lubrication of soft viscoelastic solids, J. Fluid Mech. **799**, 433 (2016).
[18] R. J. Clarke and S. Potnis, Elastohydrodynamics induced by a rapidly moving microscopic body, Proc. R. Soc. A **467**, 2852 (2011).
[19] P. Karan, J. Chakraborty, and S. Chakraborty, Influence of nonhydrodynamic forces on the elastic response of an ultra-thin soft coating under fluid-mediated dynamic loading, Phys. Fluids **32**, 022002 (2020).
[20] H. S. Davies, D. Débarre, N. El Amri, C. Verdier, R. P. Richter, and L. Bureau, Elastohydrodynamic Lift at a Soft Wall, Phys. Rev. Lett. **120**, 198001 (2018).
[21] M. E. Rosti, M. N. Ardekani, and L. Brandt, Effect of elastic walls on suspension flow, Phys. Rev. Fluids **4**, 062301(R) (2019).
[22] M. Essink, A. Pandey, S. Karpitschka, K. Venner, and J. H. Snoeijer, Regimes of soft lubrication (2020), arXiv:2007.08020.
[23] L. D. Landau and E. M. Lifshitz, *Theory of Elasticity, volume 7 of Course of Theoretical Physics* (Elsevier, New York, 1986).
[24] K. L. Johnson, *Contact Mechanics* (Cambridge University Press, Cambridge, UK, 1987).
[25] J. H. Snoeijer, J. Eggers, and C. H. Venner, Similarity theory of lubricated hertzian contacts, Phys. Fluids **25**, 101705 (2013).
[26] H. Wu, N. Moyle, A. Jagota, and C.-Y. Hui, Lubricated steady sliding of a rigid sphere on a soft elastic substrate: Hydrodynamic friction in the hertz limit, Soft Matter **16**, 2760 (2020).
[27] J. A. Greenwood, Elastohydrodynamic lubrication, Lubricants **8**, 51 (2020).
[28] B. Saintyves, T. Jules, T. Salez, and L. Mahadevan, Self-sustained lift and low friction via soft lubrication, Proc. Nat. Acad. Sci. USA **113**, 5847 (2016).
[29] Z. Zhang, V. Bertin, M. Arshad, E. Raphael, T. Salez, and A. Maali, Direct Measurement of the Elastohydrodynamic Lift Force at the Nanoscale, Phys. Rev. Lett. **124**, 054502 (2020).
[30] B. Saintyves, B. Rallabandi, T. Jules, J. Ault, T. Salez, C. Schönecker, H. A. Stone, and L. Mahadevan, Rotation of a submerged finite cylinder moving down a soft incline, Soft Matter **16**, 4000 (2020).
[31] T. Salez and L. Mahadevan, Elastohydrodynamics of a sliding, spinning and sedimenting cylinder near a soft wall, J. Fluid Mech. **779**, 181 (2015).
[32] B. Rallabandi, B. Saintyves, T. Jules, T. Salez, C. Schönecker, L. Mahadevan, and H. A. Stone, Rotation of an immersed cylinder sliding near a thin elastic coating, Phys. Rev. Fluids **2**, 074102 (2017).
[33] H. Masoud and H. Stone, The reciprocal theorem in fluid dynamics and transport phenomena, J. Fluid Mech. **879**, P1 (2019).
[34] A. Daddi-Moussa-Ider, B. Rallabandi, S. Gekle, and H. A. Stone, Reciprocal theorem for the prediction of the normal force induced on a particle translating parallel to an elastic membrane, Phys. Rev. Fluids **3**, 084101 (2018).
[35] B. Rallabandi, N. Oppenheimer, M. Ben Zion, and H. A. Stone, Membrane-induced hydroelastic migration of a particle surfing its own wave, Nat. Phys. **14**, 1211 (2018).
[36] T. G. J. Chandler and D. Vella, Validity of Winkler's mattress model for thin elastomeric layers: Beyond Poisson's ratio, Proc. R. Soc. A **476**, 20200551 (2020).
[37] J. Wang, *Interfacial Mechanics: Theories and Methods for Contact and Lubrication* (CRC Press, Boca Raton, FL, 2019).
[38] S. Leroy, A. Steinberger, C. Cottin-Bizonne, F. Restagno, L. Léger, and É. Charlaix, Hydrodynamic Interaction Between a Spherical Particle and an Elastic Surface: A Gentle Probe for Soft Thin Films, Phys. Rev. Lett. **108**, 264501 (2012).

[39] A. J. Goldman, R. G. Cox, and H. Brenner, Slow viscous motion of a sphere parallel to a plane wall—I motion through a quiescent fluid, Chem. Eng. Sci. **22**, 637 (1967).
[40] A. J. Goldman, R. G. Cox, and H. Brenner, Slow viscous motion of a sphere parallel to a plane wall—II Couette flow, Chem. Eng. Sci. **22**, 653 (1967).
[41] L. M. Milne-Thomson, *Theoretical Hydrodynamics* (Courier Corporation, Boston, MA, 1996).
[42] H. Brenner, The slow motion of a sphere through a viscous fluid towards a plane surface, Chem. Eng. Sci. **16**, 242 (1961).
[43] T. Bickel, Brownian motion near a liquid-like membrane, Eur. Phys. J. E **20**, 379 (2006).
[44] T. Bickel, Hindered mobility of a particle near a soft interface, Phys. Rev. E **75**, 041403 (2007).
[45] B. Shoelson, H. Cai, and R. S. Chadwick, Surface Green's functions for an incompressible, transversely isotropic elastic half-space, SIAM J. Appl. Math. **64**, 1186 (2004).
[46] M. Eskandari and H. M. Shodja, Green's functions of an exponentially graded transversely isotropic half-space, Int. J. Solids Struct. **47**, 1537 (2010).